Title

Multiphysics Level-Set Topology Optimization of a Rover Chassis for Extreme Cold Environments

Authors

Guibert, Alexandre T

Aaron, Kim

Daimaru, Takuro

et al.

Publication Date

2024-01-08

DOI

10.2514/6.2024-2233

Peer reviewed

AIAA SciTech Forum
8-12 January 2024, Orlando, FL
AIAA SCITECH 2024 Forum

10.2514/6.2024-2233

Multiphysics Level-Set Topology Optimization of a Rover Chassis for Extreme Cold Environments

Alexandre T. Guibert*
University of California San Diego, La Jolla, CA, 92093, USA
NASA Jet Propulsion Laboratory, California Institute of Technology, Pasadena, CA, 91011, USA

Kim M. Aaron † and Takuro Daimaru ‡
NASA Jet Propulsion Laboratory, California Institute of Technology, Pasadena, CA, 91011, USA

Sandilya Kambampati §
Intact Solutions, Inc., Madison, WI, 53703, USA

H. Alicia Kim¶
University of California San Diego, La Jolla, CA, 92093, USA

Topology optimization is applied to design a lunar rover chassis to reduce thermal losses while maintaining adequate structural strength and stiffness. Space missions in extreme cold environments, such as the permanently shadowed regions (PSR) of the moon, are designed to reduce the power needed to maintain the minimum temperature for items that cannot operate at very low temperatures, such as electronic components. Energy consumed to maintain the temperature reduces the energy that could be used to operate instruments for improved science return. Consequently, it is essential to have an efficient thermal design while preserving the integrity of the structure. Given the design freedom it offers, topology optimization is an ideal candidate for such a task. In this work, the design of a rover chassis for extreme cold environments is investigated. The chassis is topologically optimized using the level-set method and moments-based meshfree finite element analysis with thermo-mechanical loads while the mass of the chassis is constrained to obtain a lightweight design. The main advantage of moment-based meshfree simulation is that it eliminates meshing-related bottlenecks, especially for large-scale multiphysics topology optimization problems. The objective function is defined as the weighted sum of thermal compliance and structural compliance. Several sets of weights are explored and the optimized designs are compared. The proposed methodology is reusable and extensible making it well-suited for a variety of designs for future space missions in extreme environments. The simulation and optimization tools that are developed in this study are available as a part of the software package, Intact.Generative™ from Intact Solutions.

I. Nomenclature

$\phi(x)$	=	level-set function where x is a point in the design domain
Ω, Γ, $\mathcal{D}$	=	optimized domain, optimized domain boundary, design domain
Ω_e	=	finite element domain
V_n	=	design velocity field normal to the boundary defined as positive in the outward direction
Δt	=	pseudo time-step
C_s, C_t	=	structural compliance, thermal compliance
k_1, k_2	=	weights in the objective function associated with C_s and C_t respectively

*Ph.D. Student in the Structural Engineering Department at UCSD, Mechanical Engineer Academic Part-Time in the Payload & Small Spacecraft Mechanical Engineering Section at JPL, and AIAA Student Member.

†Chief Engineer for Architecture and Formulation, Payload & Small Spacecraft Mechanical Engineering Section.

‡Thermal Engineer, Advanced Thermal Concepts And Analysis.

§Research Scientist.

¶Jacobs Scholar Chair Professor, Structural Engineering Department, and AIAA Associate Fellow.

$\mathcal{J}, \xi$	=	objective function, volume fraction
$\boldsymbol{K_s^e}, \boldsymbol{K_s}$	=	element stiffness matrix, global stiffness matrix
$\boldsymbol{K_t^e}, \boldsymbol{K_t}$	=	element conductivity matrix, global conductivity matrix
$\boldsymbol{B_s}, \boldsymbol{B_t}$	=	strain displacement matrix, temperature gradient matrix
$\boldsymbol{C_s}, \boldsymbol{C_t}$	=	material stiffness tensor, convection matrix
$\boldsymbol{f_s}, \boldsymbol{f_t}$	=	mechanical load, thermal load
$\boldsymbol{u_s}, \boldsymbol{u_t}$	=	nodal displacement vector, nodal temperature vector
$\mathcal{R}_1, \mathcal{R}_2$	=	residuals of the thermal and elasticity models respectively
$w_{e,i}, m_k$	=	weight at a quadrature point i for element e, k-th moment
ψ, N_e	=	weighting function, number of quadrature points in an element e
$\hat{b} = [b_0, b_1, \dots]$	=	a basis

II. Introduction

In the next two decades, moon and Mars rover missions will play a critical role in advancing scientific knowledge. However, these environments pose great challenges to engineering. The rover chassis must be as light as possible to incorporate as many scientific instruments as possible. The chassis must be stiff enough to survive the launch and operate reliably. Finally, operating in extreme conditions implies that the primary structure must be thermally efficient. These requirements create a design space that can be difficult to navigate with counter-intuitive candidate solutions. An inverse design approach is an ideal method for such problems and can lead to time savings and better performance. Inverse design starts with desired performance goals and iterates the design to achieve the desired level of performance. Gradient-based topology optimization algorithms can utilize quantities of interest sensitivities to guide changes in the design. This is in contrast to "forward design" in which an experienced engineer selects components based on past experience. When an engineer wants to alter the performance, they modify the design and reanalyze the system. This involves more experience-based intuition rather than mathematically derived sensitivities to iterate the design.

We present a reusable methodology for topology optimization of structures for extreme cold missions. The finite element analysis is based on the quadrature rules derived from moments and is discussed in Section III. The level-set method is used as a gradient-based topology optimization method and is introduced in Section IV. Finally, the methodology is demonstrated with numerical examples presented in Section V where the optimization formulation is investigated and where the optimized designs are analyzed.

III. Moments-Based Finite Element Analysis

As a design evolves during optimization, the geometry can become difficult to analyze using a body-fitted mesh as it would require remeshing at every iteration. Remeshing can be an expensive operation and body-fitted mesh can lead to skewed elements that induce numerical errors if not carefully treated. Instead, a fixed mesh is preferred for its computational efficiency and robustness. However, a background mesh, also called an Eulerian mesh, can raise the question of the treatment of elements that are only partially overlaid by the solid domain. We remediate this issue by using the moment-vector-based simulation [1] to compute specific quadrature rules for these elements where the moment m_i is defined as

$$m_i(\psi) = \int_\Omega \psi b_i d\Omega \quad b_i \in \hat{b} \tag{1}$$

Knowing how the boundary of the geometry Γ cuts the elements of an Eulerian mesh, a linear system involving the moments of the basis functions can be solved for $w_{e,i}$. A finite element analysis can then be performed as usual using the derived quadrature rules. For example, the element matrices are computed as

$$\boldsymbol{K_s^e} = \int_{\Omega_e} \boldsymbol{B_s}^\top \boldsymbol{C_s} \boldsymbol{B_s} d\Omega = \sum_{i=1}^{N_e} w_{e,i} \boldsymbol{B_s}^\top \boldsymbol{C_s} \boldsymbol{B_s} \tag{2}$$

$$\boldsymbol{K_t^e} = \int_{\Omega_e} \boldsymbol{B_t}^\top \boldsymbol{C_t} \boldsymbol{B_t} d\Omega = \sum_{i=1}^{N_e} w_{e,i} \boldsymbol{B_t}^\top \boldsymbol{C_t} \boldsymbol{B_t} \tag{3}$$

The element matrices can be assembled to obtain $\boldsymbol{K_s}$ and $\boldsymbol{K_t}$ using the standard procedures. Then, the systems $\boldsymbol{K_s u_s} = \boldsymbol{f_s}$ and $\boldsymbol{K_t u_t} = \boldsymbol{f_t}$ are solved for $\boldsymbol{u_s}$ and $\boldsymbol{u_t}$. More details regarding moments-based finite element analysis are given in [1–3].

IV. Topology Optimization

The level set topology optimization software package, Intact.Generative, is used in this study. Intact.Generative, which utilizes moment-vector-based meshfree FEA, can solve topology optimization problems for large-scale multiphysics applications, without the need for meshing. The implementation details of Intact.Generative are briefly discussed below.

A. Level-Set Topology Optimization

The level-set topology optimization (LSTO) is a gradient-based topology optimization method where the design is unambiguously described throughout the optimization history by an implicit level-set function ϕ such that

$$\begin{cases} \phi(x) \geq 0, x \in \Omega \\ \phi(x) = 0, x \in \Gamma \\ \phi(x) < 0, x \in \mathcal{D} \setminus \Omega \end{cases} \tag{4}$$

The optimized domain is iteratively updated via the Hamilton-Jacobi equation, so-called the level-set equation

$$\frac{d\phi(x)}{dt} + |\nabla\phi(x)|V_n(x) = 0 \tag{5}$$

The design velocity field drives the optimization and is computed via a linearized sub-optimization problem [4]. The quantity $|\nabla\phi(x)|$ is computed using the Hamilton-Jacobi weighted essentially non-oscillatory scheme (HJ-WENO) [5]. More details regarding the LSTO method can be found in [3, 6–8]

B. Optimization Formulation

The objective function of the optimization problem is the weighted sum of the thermal and structural compliance normalized by their respective initial values at each stage, i.e.,

$$\mathcal{J} \triangleq k_1 \frac{C_s}{C_{s0}} + k_2 \frac{C_t}{C_{t0}} \tag{6}$$

where a stage is defined by a given number of iterations. Structural and thermal compliances are defined as $C_s = \boldsymbol{f_s}^\top \boldsymbol{u_s}$ and $C_t = \boldsymbol{f_t}^\top \boldsymbol{u_t}$, respectively. Stages of 20 iterations are chosen for this work. The discretization, defined as a level, is refined every 6 stages for this work, i.e., the finite element (FE) edge size is decreased every 120 iterations. To illustrate the concept of levels and stages, in a case where 2 levels of 5 stages are used, there would be 10 stages for a total of 200 optimization iterations as shown in Fig.1. For this work, 3 levels of 6 stages each are used.

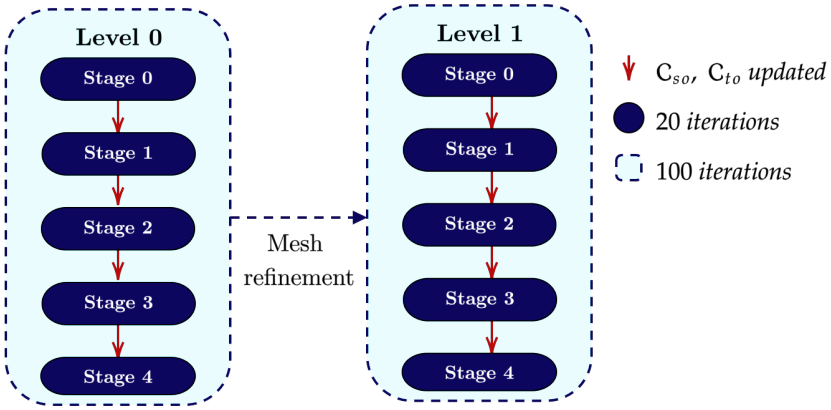

Fig. 1 Example of 2 levels with 5 stages each for optimization

Additionally, the volume for the optimized component is constrained such that a fraction ξ of the design domain is prescribed. The volume fraction ξ is sequentially decreased at each stage, the details are given for each numerical example in the next Section. Finally, the optimization problem to be solved can be expressed as

$$\begin{aligned} \min_{\Omega} \quad & \mathcal{J} \\ \text{subject to} \quad & \text{Vol}(\Omega) \leq \xi \, \text{Vol}(\mathcal{D}) \\ & \mathcal{R}_i = 0, \quad i = 1, 2 \end{aligned} \tag{7}$$

V. Numerical examples

A. Set up and Boundary Conditions

The design domain dimensions and interfaces to the rover's main components are adopted from the Intrepid planetary mission concept [9]. The design domain, along with its overall dimensions and connections to other components, is illustrated in Fig. 2. For the rover chassis, the materials under consideration for the mission are Titanium and Aluminum, which are to be additively manufactured. To analyze the system, the required thermal and structural material properties for the heat conduction and linear elasticity models are listed in Table 1.

Table 1 Properties for the thermo-mechanical analysis

Property	Titanium	Aluminum
Thermal conductivity [W/m.K]	7.3	220
Young's modulus [GPa]	110	68
Poisson's ratio [-]	0.31	0.32

The mobility interfaces are treated as heat sinks, with no displacements allowed in any direction. At the mast interface, a traction load equal to the mast's weight is applied. Similarly, at the electronics interface, a traction load corresponding to the combined weight of batteries and electronic components is applied, and in addition, a heat flux boundary condition due to the batteries and electronics heating is also applied. The mast is assumed to have a mass of 60 kg, while the batteries and electronics have a combined mass of 85 kg. Earth gravity which is more conservative than the gravity on the moon is used since the chassis should be transported and manufactured on Earth. The heat flux applied at the electronics interface is 91 W/m^2.

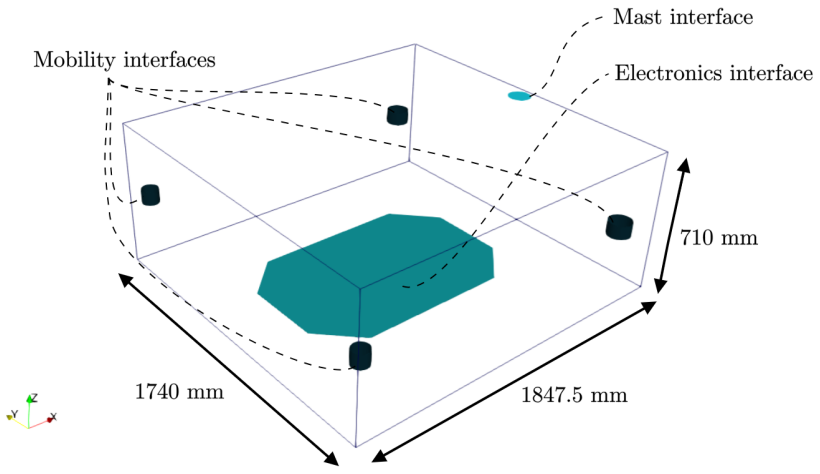

Fig. 2 Design domain and its interfaces

B. Results

In this study, we explore the optimization of a system with three distinct sets of weights and two materials, Aluminum and Titanium, while varying three different volume fractions, denoted as ξ. The sets of weights were chosen arbitrarily, based on preliminary tests. To investigate the effects of individual parameters, we adopt the One Factor at a Time (OFAT) strategy, resulting in a total of 18 cases. The specifics for all cases are provided in Table 2. For each case, we present the final designs in Appendix A. The convergence histories for the cases that lead to connected designs, namely cases 1, 2, 3, 7, 10, 11, 12, 16, and 17, are shown in Fig.3. We observe that the inequality volume constraint is active. Additionally, we note that the values of both thermal and structural compliances exhibit oscillatory behavior in cases 1 and 10, while cases 2 and 11 also show some oscillations in structural compliance. These particular cases are associated with relatively low volume fractions, and they represent the minimum weight magnitude considered in this study for thermal compliance.

Table 2 Cases studied

Case	Material	k_1	k_2	Level 0^a - ξ	Level 1^b - ξ	Level 2^c - ξ
1, 2, 3	Aluminum	1	-0.01	20 %	5 %	2 %, 3 %, 5 %
4, 5, 6	Aluminum	1	-0.02	20 %	5 %	2 %, 3 %, 5 %
7, 8, 9	Aluminum	1	-0.04	20 %	5 %	2 %, 3 %, 5 %
10, 11, 12	Titanium	1	-0.01	20 %	5 %	2 %, 3 %, 5 %
13, 14, 15	Titanium	1	-0.02	20 %	5 %	2 %, 3 %, 5 %
16, 17, 18	Titanium	1	-0.04	20 %	5 %	2 %, 3 %, 5 %

[a]The FE edge size is 20 mm and the edges of the level-set cells is 10 mm
[b]The FE edge size is 12 mm and the edges of the level-set cells is 6 mm
[c]The FE edge size is 8 mm and the edges of the level-set cells is 4 mm

C. Evaluation of the optimized topologies

We can now analyze the optimized topologies using moments-based finite element analysis for linear elasticity and heat conduction with the finest mesh, i.e., with a FE edge size of 8 mm. The mass, maximum displacement magnitude, maximum von Mises stress, and maximum temperature increase are shown in Table 3. Note that the disconnected designs are disregarded and thus 9 cases are to be evaluated.

We observed that all the cases investigated in Table 3 exhibited a maximum displacement of less than 1 mm. Additionally, the maximum von Mises stress recorded was 1.094 MPa. As both Aluminum and Titanium have a maximum yield stress that is at least two orders of magnitude greater than these observed values, the structural loads do not pose any threat to the integrity of the chassis. In fact, the factor of safety is greater than a hundred, providing a significant margin of safety. Given these structural considerations, our focus will now shift toward the crucial elements of extreme cold missions: the chassis temperature increase and its mass. It is worth noting that although the structural quantities will not be critical in comparing the designs, including them as either objectives or constraints is essential to prevent trivial solutions for thermal insulation problems such as disconnected heat fluxes and heat sink boundaries.

Fig.4 presents the relationship between the temperature increase and the mass of the chassis, allowing us to further examine the optimized designs. Titanium emerges as more effective in terms of mass for achieving temperature increase, with cases 10 and 16 showing the most promising results in terms of thermal performance. This result aligns with our expectations, given that Titanium has a thermal conductivity over 30 times lower than that of Aluminum. For Aluminum, cases 1 and 7 are the most promising due to their low weight and significant temperature increase. The temperature increases for cases 1 and 10 are shown in Fig.5. Notably, the thermal performance and mass of the chassis are primarily influenced by the volume fraction and the choice of material. Indeed, similar results are obtained for both $k_2 = -0.01$ and $k_2 = -0.04$, with slightly better thermal performance observed for $k_2 = -0.01$. Thus, for future studies, we will adopt the value of $k_2 = -0.01$ as our preferred option.

The moon's permanently shadowed regions (PSR) can experience temperatures below 110 K [10], while certain electronics require temperatures at or above 273 K to function properly. Consequently, we must achieve a temperature

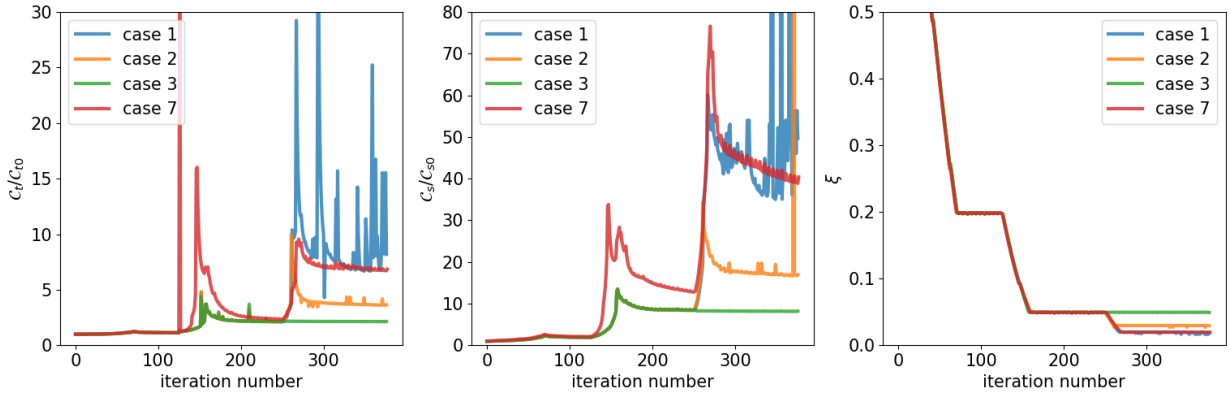

(a) Cases with Aluminum

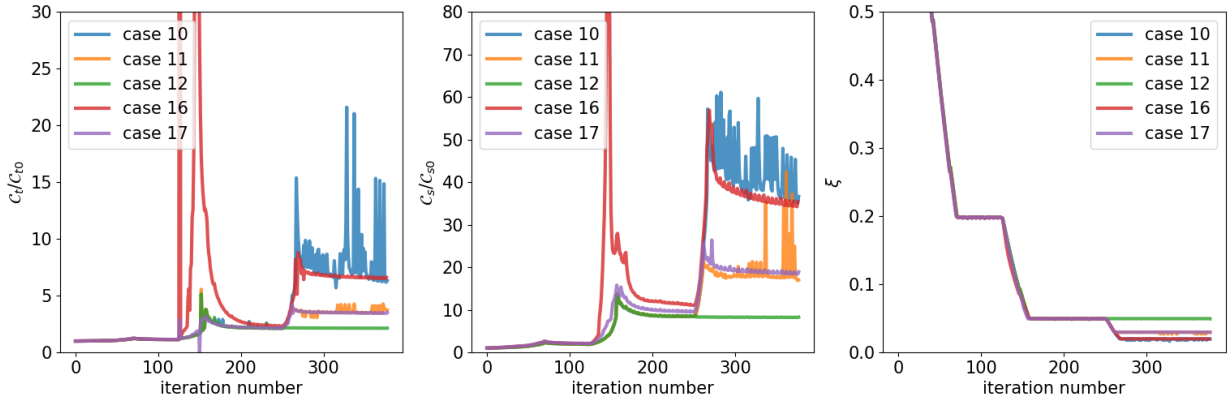

(b) Cases with Titanium

Fig. 3 Convergence histories of thermal compliance, structural compliance, and volume fraction (from left to right) for the cases with connected final topologies

increase of at least 163 K in the electronics region compared to the external temperature. In addition to thermal requirements, it is a deliberate design choice to keep the rover's mass at 100 kg or below. This constraint ensures that the rover can carry as much scientific equipment as possible while maintaining a manageable total mass. To meet these critical objectives, our ideal scenario is to combine the low mass of case 1 with the substantial temperature increase seen in case 10, or ideally, even better performance. Achieving this balance requires reducing the volume fraction further, aiming for a value around 1 % which will be the object of future work. However, it is important to acknowledge that achieving such a low volume fraction will introduce new challenges. Thin members are more susceptible to buckling, necessitating careful consideration of additional structural stability in the optimization formulation.

Table 3 Evaluation of the optimized topologies

Case	Mass[a] [kg]	u_{max}[b] [mm]	$\sigma_{vM,max}$[c] [MPa]	ΔT_{max}[d] [K]
1	106.7	0.0198	0.645	69.89
2	172.8	0.0100	0.295	24.69
3	288.0	0.0065	0.170	12.37
7	114.5	0.0191	0.541	57.91
10	190.3	0.0099	0.497	158.3
11	287.5	0.0065	0.274	74.66
12	479.9	0.0041	0.217	37.45
16	191.7	0.0109	0.491	153.5
17	286.2	0.0069	1.094	82.74

[a]Density of aluminum and titanium are taken as 2.7 g/cm^3 and 4.5 g/cm^3
[b]Maximum displacement magnitude
[c]Maximum von Mises stress
[d]Maximum temperature increase

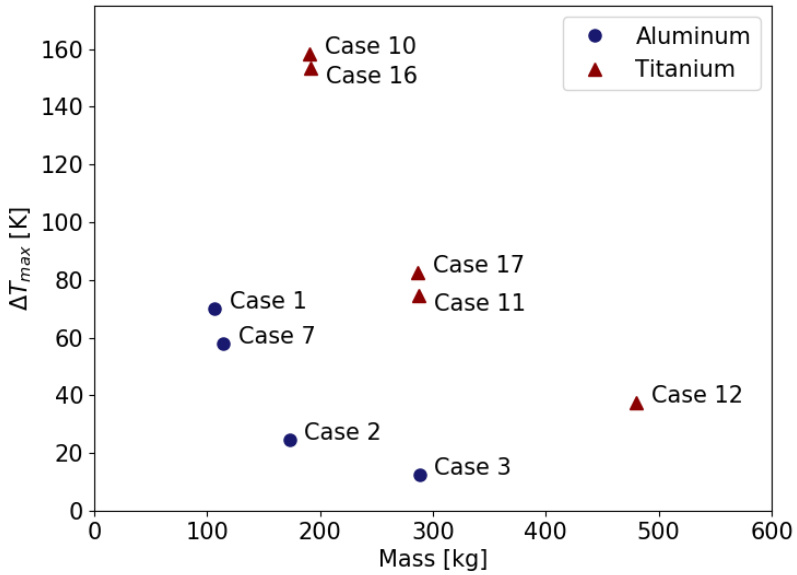

Fig. 4 Temperature increase as a function of the mass of the chassis

VI. Conclusions

In conclusion, this work presents a study on topology optimization of a rover chassis using the level set topology optimization method in conjunction with moments-based finite element analysis where the dimensions and interfaces of the design domain were derived from the Intrepid planetary mission concept. The simulation and optimization tools that are developed in this study are available as a part of the topology optimization software package, Intact.Generative. Throughout the study, two potential materials, Titanium and Aluminum, were evaluated for additive manufacturing of the chassis. The steady-state heat conduction and linear elasticity models were employed to analyze the thermal

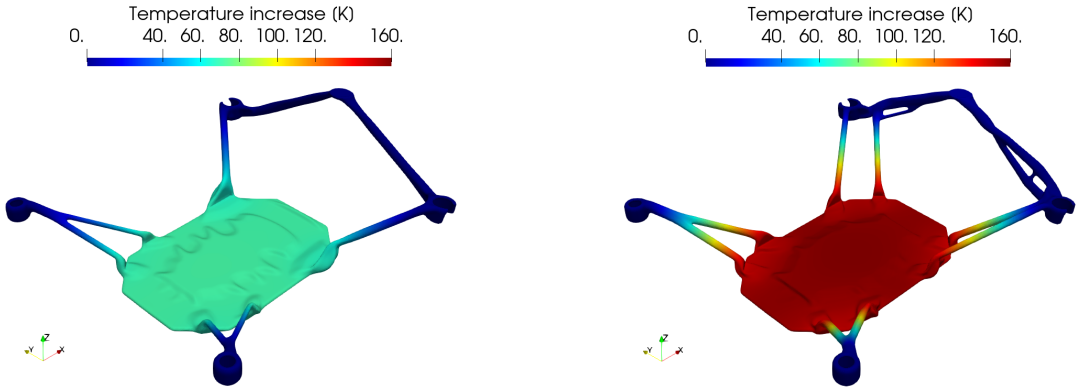

(a) Case 1 **(b) Case 10**

Fig. 5 Temperature distribution for cases 1 and 10

and structural behavior of the chassis. The results from the level set topology optimization provided valuable insights into the optimal configuration of the rover chassis, and the achievable thermal and structural performances during the planetary missions. For operational cases, structural quantities appeared to be not decisive for design selection but needed for optimization to avoid non-physical solutions. The weight given to the thermal objective was investigated with one weight, -0.01, selected for future studies. In addition, we observed that Titanium is better suited for addressing temperature increases, while Aluminum is more appropriate for achieving mass reduction. The results were promising, but further work is required to reduce the volume fraction to meet the requirements of future missions. This reduction could lead to extremely thin members that may be prone to buckling, necessitating an additional constraint consideration.

The integration of the level set topology optimization method and moments-based finite element analysis proved to be an effective approach for eliminating meshing and post-processing bottlenecks related to the optimization of the rover's chassis for improved functionality and performance. The findings from this research serve as a step forward in the field of rover design, contributing to the advancement of planetary exploration and paving the way for future missions with highly optimized rover platforms.

Future work will include exploring alternative materials for additive manufacturing to further optimize the rover's structural integrity and thermal properties. Additionally, scaled prototypes of the optimized designs will be additively manufactured and experimentally tested. Finally, dynamic simulations and buckling analyses will be incorporated to understand the chassis' response to varying terrains and launch conditions. These research efforts hold the potential to enhance the rover's performance, opening up new frontiers in planetary research.

Acknowledgments

This work was funded by the National Aeronautics and Space Administration (NASA); Part of this research was carried out at the Jet Propulsion Laboratory, California Institute of Technology, under a contract with NASA. The authors are grateful for funding for the project and Intact Solutions, Inc. for the software.

Clearance number: CL#23-6673

References

[1] Taber, A., Kumar, G., Freytag, M., and Shapiro, V., "A moment-vector approach to interoperable analysis," *Computer-Aided Design*, Vol. 102, 2018, pp. 139–147.

[2] Kumar, G., and Taber, A., "An integral representation of fields with applications to finite element analysis of spatially varying materials," *Computer-Aided Design*, Vol. 126, 2020, p. 102869.

[3] Kambampati, S., Taber, A., Kumar, G., and Kim, H. A., "A CAD-aware plug-and-play topology optimization framework using moments," *Structural and Multidisciplinary Optimization*, Vol. 66, No. 3, 2023, p. 63.

[4] Dunning, P. D., and Kim, H. A., "Introducing the sequential linear programming level-set method for topology optimization," *Structural and Multidisciplinary Optimization*, Vol. 51, 2015, pp. 631–643.

[5] Liu, X.-D., Osher, S., and Chan, T., "Weighted essentially non-oscillatory schemes," *Journal of computational physics*, Vol. 115, No. 1, 1994, pp. 200–212.

[6] Sivapuram, R., Dunning, P. D., and Kim, H. A., "Simultaneous material and structural optimization by multiscale topology optimization," *Structural and multidisciplinary optimization*, Vol. 54, 2016, pp. 1267–1281.

[7] Hyun, J., Jauregui, C., Kim, H. A., and Neofytou, A., "On development of an accessible and non-intrusive level-set topology optimization framework via the discrete adjoint method," *AIAA SCITECH 2022 Forum*, 2022, p. 2548.

[8] Sethian, J. A., and Vladimirsky, A., "Fast methods for the Eikonal and related Hamilton–Jacobi equations on unstructured meshes," *Proceedings of the National Academy of Sciences*, Vol. 97, No. 11, 2000, pp. 5699–5703.

[9] Elliott, J. O., and Robinson, M., "Intrepid Planetary Mission Concept Overview," *Jet Propulsion Laboratory*, 2020.

[10] Bickel, V. T., Moseley, B., Hauber, E., Shirley, M., Williams, J.-P., and Kring, D. A., "Cryogeomorphic characterization of shadowed regions in the Artemis exploration zone," *Geophysical Research Letters*, Vol. 49, No. 16, 2022, p. e2022GL099530.

Appendix A - Isometric views of optimized topologies for the 18 cases considered

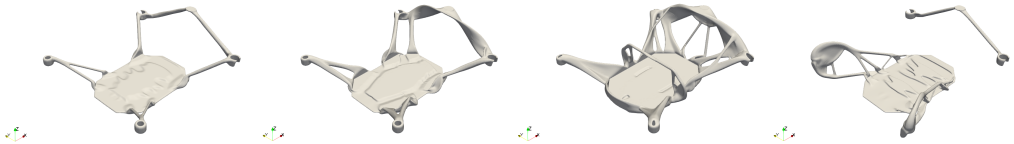

(a) case 1 (b) case 2 (c) case 3 (d) case 4

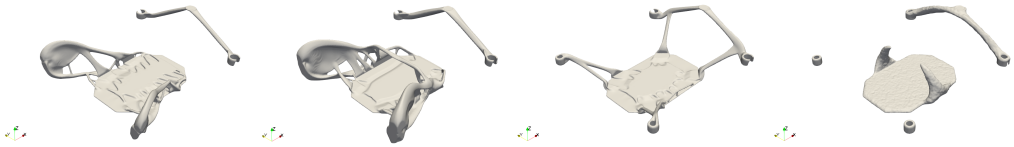

(e) case 5 (f) case 6 (g) case 7 (h) case 8

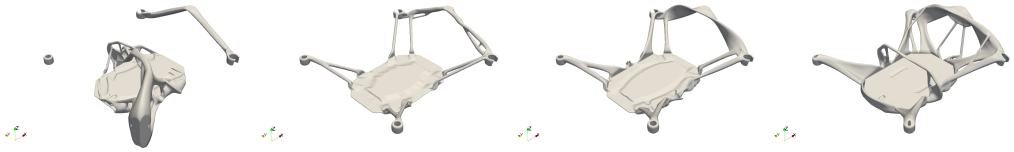

(i) case 9 (j) case 10 (k) case 11 (l) case 12

(m) case 13 (n) case 14 (o) case 15 (p) case 16

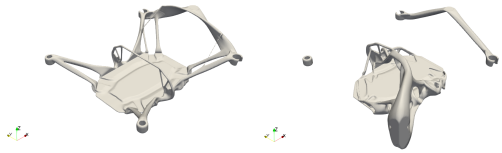

(q) case 17 (r) case 18